Petroleum Science 23 (2026) 7207–7215

Contents lists available at ScienceDirect

Petroleum Science

journal homepage: www.keaipublishing.com/en/journals/petroleum-science

Original Paper

A fluidic hammer as a high-fidelity seismic-while-drilling source: A direct, quantitative comparison with conventional drill bits

Bo-Yao Zhang [a,b], Jian-Ming Peng [a,b], Dong Ge [a,b,*]

[a] Key Laboratory of Geophysical Exploration Equipment, Ministry of Education, Jilin University, Changchun, 130026, Jilin, China
[b] College of Construction Engineering, Jilin University, Changchun, 130026, Jilin, China

ARTICLE INFO

Article history:
Received 14 November 2025
Received in revised form
23 December 2025
Accepted 11 June 2026
Available online 16 June 2026

Edited by Jia-Jia Fei

Keywords:
Fluidic hammer
Seismic-while-drilling (SWD)
Seismic source characterization
Source comparison
Drill-bit seismology
Percussion-rotary drilling

ABSTRACT

We performed a direct comparative analysis of the seismic wavefields radiated from three distinct drilling mechanisms under controlled laboratory conditions: percussion-rotary drilling with a fluidic hammer, and conventional rotary drilling with roller-cone and polycrystalline-diamond-compact (PDC) bits. The results reveal the comprehensive superiority of the fluidic hammer. A quantitative analysis of the peak signals indicates that the fluidic hammer radiates approximately 12.2 times more seismic energy than the roller-cone bit and over 809.3 times more than the PDC bit. Further analysis demonstrates that the fluidic hammer produces a high-energy and broadband (50–150 Hz) wavefield. The kinematic fidelity of this wavefield was robustly validated against an independent benchmark experiment using a traditional instrumented hammer source. Its highly repeatable wavelet and unwavering kinematic response across all energy levels cement its status as a truly high-fidelity source. Crucially, its energy output exhibits a strong linear relationship ($R^2 = 0.9360$) with the operational flow rate, proving the source is quantitatively controllable. These findings demonstrate that the fluidic hammer source mechanism can overcome the fundamental energy and stability limitations of traditional drill-bit seismic-while-drilling (DB-SWD), offering a promising pathway toward high-fidelity, quantitative subsurface imaging.

© 2026 The Authors. Publishing services by Elsevier B.V. on behalf of KeAi Communications Co. Ltd. This is an open access article under the CC BY-NC-ND license (http://creativecommons.org/licenses/by-nc-nd/4.0/).

1. Introduction

Real-time subsurface imaging during drilling is a critical capability that enhances safety and efficiency in energy exploration and geotechnical engineering (Poletto and Miranda, 2004). A key technology enabling this is seismic-while-drilling (SWD), which broadly includes drill-bit SWD (DB-SWD) and VSP-while-drilling (VSP-WD) (Zhang et al., 2022). Among these, DB-SWD utilizes the vibrations generated by the drill bit impacting the formation as a downhole source to acquire data analogous to a reverse vertical seismic profile (RVSP) without halting drilling operations (Haldorsen et al., 1995; Zhang et al., 2022). This provides a continuous stream of information invaluable for look-ahead-of-the-bit imaging, real-time time-depth conversion, and geosteering (Jiang, 2004; Su et al., 2010).

Traditional DB-SWD relies on conventional rotary drill bits, but both primary types—roller-cone and polycrystalline-diamond-compact (PDC) bits—present significant challenges. The roller-cone bit has been proven as an adequate seismic source in numerous field applications (Haldorsen et al., 1995; Miranda et al., 1996; Naville et al., 2004; Soma et al., 2004; Zhou et al., 2015). Through its axial impact and cutting forces, it generates both compressional and shear waves (Rector and Hardage, 1992). Notwithstanding its utility, its signal originates from a pseudo-random series of tooth indentations, creating a wavefield that is inherently uncontrollable and time-variant (Poletto, 2005). The problem is exacerbated by the widespread application of PDC bits in modern drilling (Zhang et al., 2022). While highly efficient for drilling (Brett et al., 1990), their shearing mechanism is seismically quiet (Sun et al., 2015). The axial vibration forces from a PDC bit are typically more than an order of magnitude lower than those from a roller-cone bit (Poletto, 2005). Consequently, SWD data acquired with PDC bits are often characterized by poor quality and a low signal-to-noise ratio (SNR), a limitation widely reported in various

* Corresponding author.
E-mail address: gedong12593@jlu.edu.cn (D. Ge).
Peer review under the responsibility of China University of Petroleum (Beijing).

https://doi.org/10.1016/j.petsci.2026.06.021
1995-8226/© 2026 The Authors. Publishing services by Elsevier B.V. on behalf of KeAi Communications Co. Ltd. This is an open access article under the CC BY-NC-ND license (http://creativecommons.org/licenses/by-nc-nd/4.0/).

environments (Anchliya, 2006; Miranda et al., 1999; Zhang et al., 2022). The inherent weaknesses of these sources lead to multiple downstream issues, for instance, they create significant signal processing challenges; the reliance on a pilot signal that is heavily distorted by the drill string's transmission effects (including attenuation, time delays, and filtering) severely degrades the quality of the final processed data and compromises imaging reliability (Rector, 1990).

An emerging approach to overcome this bottleneck is to leverage impact-based drilling tools, which are inherently more energetic, as superior seismic sources. A key example is the fluidic hammer, a percussion drilling tool recognized for its high rate of penetration in hard formations (Ge et al., 2022). It utilizes an internal fluidic oscillator to cyclically direct high-pressure fluid, driving an impact body to strike the drill bit, thus generating powerful, periodic impacts. Previous work has demonstrated the potential of percussion drills to generate strong signals suitable for SWD (Reppert, 2013; Yokota et al., 2004). Field studies have further confirmed that systems like reverse-circulation (RC) percussion drilling can produce high-energy, wideband signals ideal for seismic imaging (Sun et al., 2015). More recently, the capabilities of SWD have been further extended, with studies utilizing percussion sources for drill-bit positioning (Wilczynski et al., 2023) and developing advanced denoising algorithms to address signal fidelity challenges (Birnie et al., 2024).

While previous studies have highlighted the potential of various impact-based sources, a systematic, quantitative comparison between the seismic signals generated by a fluidic hammer and those from conventional rotary bits under controlled laboratory conditions had not been performed. This study aims to fill this gap by performing the first direct, side-by-side comparison of these three source mechanisms under controlled laboratory conditions. First, we provide a direct comparison of the radiated energy to establish the fluidic hammer's performance advantages. Subsequently, we conduct an in-depth characterization of the fluidic hammer's seismic records to demonstrate their quality and utility. Through these analyses, we evaluate its key source attributes: the production of a high-energy, broadband, and stable wavefield; the precise controllability of its energy output as a function of operational parameters; and the signal's suitability for formation velocity inversion. By combining this comparative analysis with an in-depth characterization, our study provides a robust, evidence-based evaluation of the fluidic hammer as a high-fidelity source, whose performance and kinematic accuracy are validated through both direct comparison and an independent benchmark experiment, for the next generation of quantitative SWD.

2. Methodology

We conducted a series of systematic laboratory experiments to quantitatively characterize and compare the physical properties of three distinct while-drilling seismic sources.

2.1. Experimental setup and geometry

The laboratory experiments were designed to directly compare the seismic signals generated by three distinct source mechanisms. The overall experimental system consists of three main components: the seismic source generation unit, a geophone array, and a data acquisition system (Fig. 1(a)).

The primary source investigated was an SC86-H fluidic hammer, driven by a high-pressure triplex pump. Its main

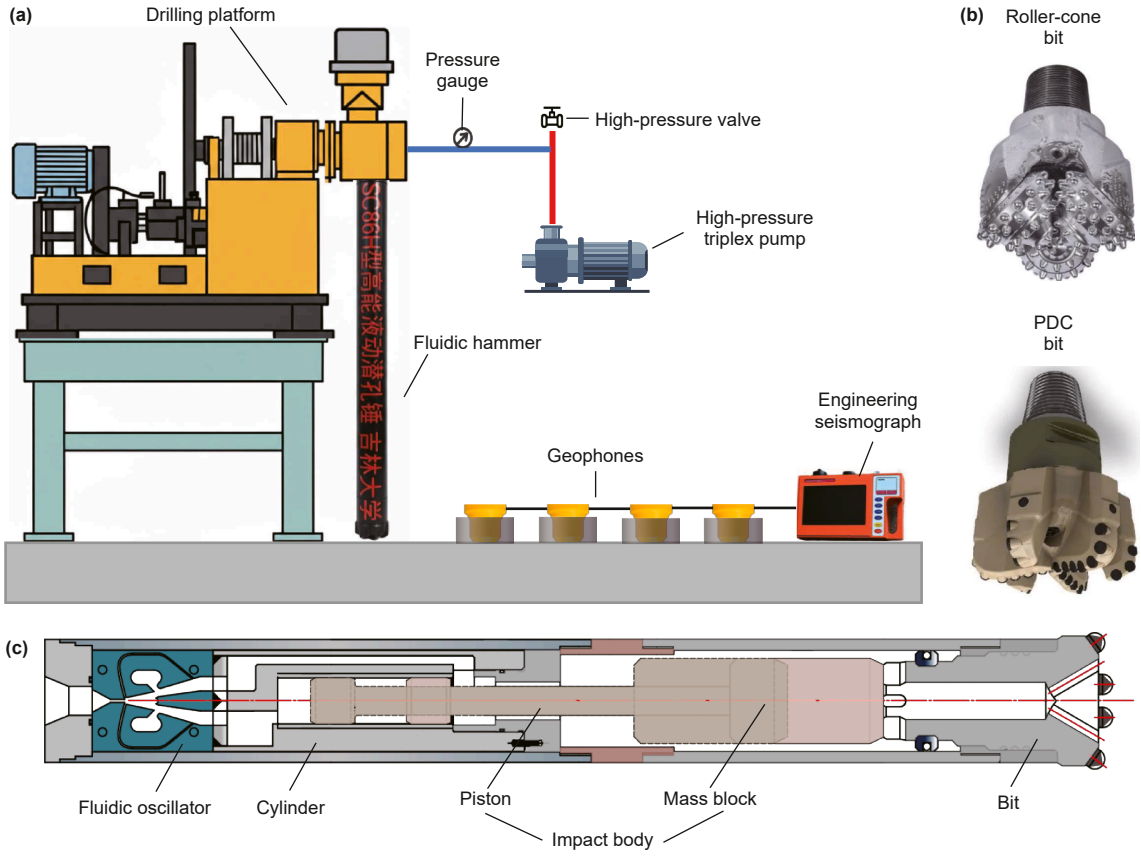


Fig. 1. Experimental setup and seismic sources. (**a**) Schematic of the laboratory experimental system. (**b**) Photographs of the conventional roller-cone and PDC bits used for comparison. (**c**) Cross-sectional diagram of the SC86-H fluidic hammer detailing its internal components.

Table 1
SC86-H specifications.

Specifications	Values
Mass of the impact body, kg	8
Drill bit diameter, mm	95
Full stroke length, mm	110
Impact frequency, Hz	8–13
Impact energy, J	50–100

specifications are listed in Table 1. Its operation is governed by an internal fluidic oscillator that drives an impact body to periodically strike the drill bit, generating powerful seismic signals (Fig. 1(c)). For the comparative tests, two conventional rotary drilling bits were used: a roller-cone bit and a PDC bit (Fig. 1(b)). To ensure a fair comparison, all three source configurations utilized a 95 mm diameter drill bit (a button bit for the fluidic hammer), and a constant weight-on-bit (WOB) of 15 kN, chosen to ensure sufficient coupling while preserving the integrity of the concrete test block, was applied and maintained via the rig's hydraulic loading system throughout the experiments. The rotational speeds were selected based on the distinct working mechanisms of the tools: 60 RPM was maintained for the PDC and roller-cone bits to ensure effective cutting action, while a lower speed of 15 RPM was selected for the fluidic hammer, as its primary breaking mechanism is vertical impact, with rotation serving only to index the bit buttons. For the baseline comparison, the roller-cone and PDC bits were operated solely under these specified conditions, while the fluidic hammer was tested across a range of energy levels. During operation, each of the three sources was vertically and rigidly coupled to the concrete floor to ensure efficient energy transmission.

Seismic signals were acquired using four vertical-component geophones (10 Hz natural frequency). To characterize the source performance across different propagation distances, two complementary linear survey layouts were implemented with the source fixed at the 0-m mark: a near-to-mid field layout (geophones at 1, 4, 7, and 10 m) and a far-field large-offset layout (geophones at 1, 10, 20, and 30 m).

In addition to the comparative tests, a separate benchmark experiment was conducted to independently validate the kinematic data. This experiment utilized an instrumented hammer with an external trigger switch as the seismic source. The hammer strike provided a precise zero-time reference, allowing for the direct measurement of absolute travel times. The geophone layout and data acquisition parameters for this benchmark test were kept identical to the primary experiments to ensure a direct and fair comparison.

2.2. Data acquisition

Data were acquired using a Miniseis24 engineering seismograph. For this experiment, the sampling interval was uniformly set to 0.1 ms (corresponding to a 10,000 Hz sampling rate), with 20,000 samples recorded for a total length of 2 s for each trace.

For each measurement, the respective source was activated and allowed to reach a stable operating state. The seismograph was then initiated using a self-triggering mode to continuously record 2 s of data. Four distinct source energy levels were investigated by setting the pump flow rate to 100, 140, 180, and 220 L/min for each of the two geophone layouts.

For the separate benchmark experiment, data acquisition was performed using an external trigger mode. The trigger signal was generated directly by the instrumented hammer's switch upon impact, providing a precise zero-time reference for the recordings. All other acquisition parameters, including the seismograph, sampling rate, and record length, were kept identical to the primary experiments to ensure a fair comparison.

2.3. Data processing and analysis

The acquired multi-channel data were processed and analyzed using the following standard workflow.

(1) Signal and spectral analysis: Raw waveforms were first inspected to assess data quality. Subsequently, a rectangular window was applied to preserve the signal's transient features, and a fast Fourier transform (FFT) was applied to each trace to compute its amplitude spectrum (Bracewell, 2000), which was used to characterize the source's bandwidth and dominant frequency.
(2) Signal-to-noise ratio (SNR) analysis: To quantitatively evaluate and compare the signal quality across different offsets and source energy levels, the SNR was calculated for each trace. To establish a consistent and unbiased benchmark for comparison, a definitive background noise signature was first identified by recording a dedicated trace of ambient noise with all experimental equipment turned off. The standard deviation of this 50-sample window ($\sigma_{\text{noise_ref}}$) was computed and used as a unified noise reference for all subsequent calculations.

The SNR for each trace was then defined in decibels (dB) as (Stein and Wysession, 2009):

$$\text{SNR (dB)} = 20 \cdot \log_{10}\left(\frac{A_{\text{signal}}}{\sigma_{\text{noise_ref}}}\right)$$

where A_{signal} is the maximum absolute amplitude of the entire signal trace. This unified-noise approach ensures that the calculated SNR values directly reflect the true signal strength relative to a common baseline, allowing for a robust and physically meaningful comparison of the source's performance under varying operational parameters and at different propagation distances.

(3) Peak energy quantification: The peak energy was quantified as the square of the maximum absolute amplitude found within the entire signal trace. This approach is consistent with the signal amplitude determination used for the SNR analysis.
(4) Repeatability and kinematic analysis: The standard cross-correlation method was employed to quantitatively assess the source's high degree of repeatability and to precisely determine the relative travel times for subsequent kinematic analysis (Aki, 1957; Bendat and Piersol, 2000). The cross-correlation function $R_{xy}(\tau)$ between two discrete time-series signals, $x[n]$ (the reference trace) and $y[n]$ (a subsequent trace), is defined as:

$$R_{xy}(\tau) = \sum_{n} x[n]y[n+\tau]$$

where τ represents the time lag. The function measures the similarity between the two signals as a function of this lag. For a highly stable source like the fluidic hammer, this function exhibits a sharp, unambiguous peak. The time lag τ at which this peak occurs corresponds directly to the seismic travel-time difference between the two sensor locations. For the fluidic hammer, a 100 ms reference wavelet was selected from the 1 m trace. This duration was determined to be optimal as it is sufficient to encapsulate the

entire first impact signature while excluding subsequent reverberations or impacts, ensuring a clean and representative template for correlation. It is acknowledged that surface-based recordings include surface waves. However, due to the high velocity of the concrete medium, the direct P-wave arrives significantly earlier than the surface waves. By focusing the quantitative analysis on the high-energy first-arrival window (the first 100 ms), the study effectively isolates the direct body-wave energy from the later-arriving surface wave interference. This dual-purpose analysis provides quantitative confirmation of the source's exceptional stability and yields robust travel-time data for the velocity analysis.

3. Results

3.1. Macroscopic comparison of source performance

To first establish a macroscopic baseline of source performance, the seismic signals generated by the three drilling mechanisms were directly compared under identical laboratory conditions. The recorded time-domain waveforms reveal fundamentally different characteristics. The fluidic hammer produces a series of high-amplitude, highly repetitive, and periodic impulsive events characteristic of a stable and energetic source. In contrast, the signals from the roller-cone bit and the PDC bit exhibit significantly lower amplitudes and random, non-periodic behavior. It is worth noting that while the PDC bit exhibits a quasi-periodic signature (see inset in Fig. 2(c)), this is attributed to the blade-passing frequency inherent to rotary drilling. However, unlike the fluidic hammer's high-energy impact periodicity, the PDC signal is predominantly characterized by low-amplitude shearing noise, resulting in a significantly lower SNR.

To quantitatively assess the vast difference in radiated energy, the peak energy of each source signal was calculated and compared, as summarized in Fig. 3. The analysis confirms the overwhelming energy advantage of the fluidic hammer. Specifically, the fluidic hammer radiates approximately 12.2 times more peak seismic energy than the roller-cone bit and over 809.3 times more than the PDC bit. This result provides direct, quantitative evidence of its superior performance as a high-energy downhole seismic source.

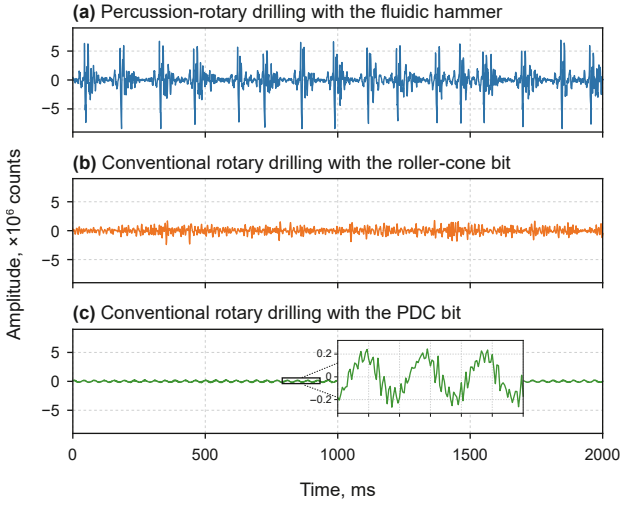


Fig. 2. Comparison of seismic waveforms recorded from the three source mechanisms. The plots share a unified amplitude axis to illustrate the significant disparity in signal strength. (**a**) Percussion-rotary drilling with the fluidic hammer. (**b**) Conventional rotary drilling with the roller-cone bit. (**c**) Conventional rotary drilling with the PDC bit; the inset provides a magnified view of the low-amplitude waveform.

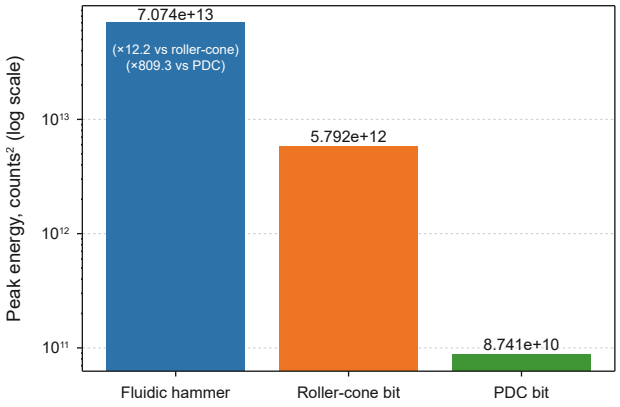


Fig. 3. Quantitative comparison of peak radiated energy from the three seismic sources. The peak energy is calculated as the square of the maximum absolute amplitude of the signal. The vertical axis is presented on a logarithmic scale to accommodate the large dynamic range.

3.2. Comparative analysis of signal characteristics

Beyond the significant energy disparity, the intrinsic characteristics of the radiated wavefields were further compared. The amplitude spectra of the three sources, calculated from the nearest offset (1 m), are shown in Fig. 4. The fluidic hammer exhibits a distinct, high-energy broadband signature, with most of its energy concentrated between 50 and 150 Hz. This distinctive high-frequency content is physically attributed to the impulsive nature of the source: The high-velocity impact of the steel piston against the bit generates a sharp, short-duration wavelet, resulting in a broadband spectral response significantly higher than the low-frequency shearing noise typical of rotary drilling. In contrast, the spectra for both the roller-cone and PDC bits show substantially lower amplitudes across all frequencies and lack a well-defined, dominant frequency band.

The stability and repeatability of the source wavelet are critical for advanced seismic processing. To evaluate this, a cross-correlation analysis was performed for each source, using the first 100 ms of the 1 m signal—a duration sufficient to encapsulate the entire first impact signature—as a reference template to correlate against the signal at a 4 m offset (Fig. 5). The fluidic

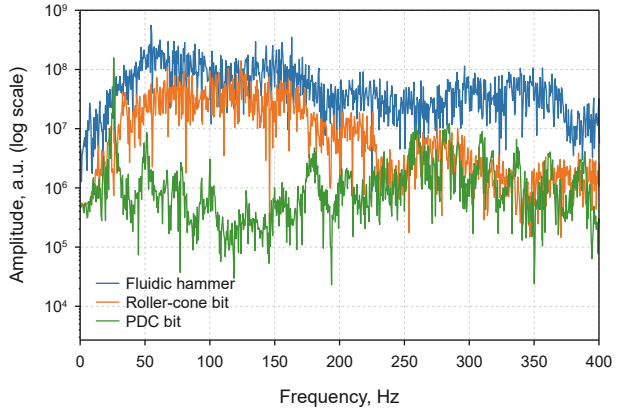


Fig. 4. Comparative amplitude spectra of the three seismic sources. Spectra were calculated from the first channel (1 m offset) of each respective dataset. The vertical axis is presented on a logarithmic scale.

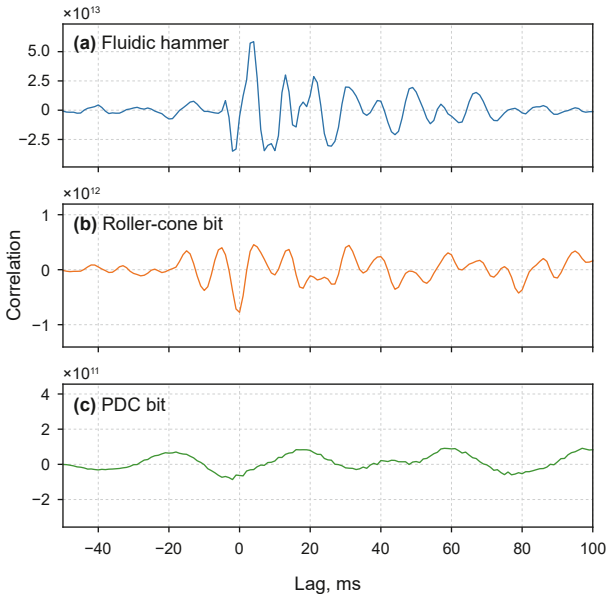


Fig. 5. Comparative analysis of signal stability and repeatability. Each panel displays the cross-correlation between the signal from the 4 m offset and a reference wavelet from the 1 m offset for each source type. (**a**) Fluidic hammer. (**b**) Roller-cone bit. (**c**) PDC bit.

hammer yields a sharp, high-amplitude correlation peak, demonstrating high wavelet coherence and fidelity during propagation. The roller-cone bit produces a much broader and less distinct peak, suggesting a less stable and predictable wavelet. For the PDC bit, the correlation function is dominated by noise with no discernible peak, confirming its pseudo-random signal character.

These superior characteristics in energy and stability directly translate to a higher SNR over distance (Fig. 6). The fluidic hammer maintains the highest SNR at all offsets, decaying slowly from approximately 59 dB at 1 m. The roller-cone bit begins with a lower SNR that also attenuates with distance. The data for the PDC bit shows a significantly lower initial SNR which decays sharply, demonstrating its limited effective range for seismic acquisition.

3.3. Physical fidelity validation of the fluidic hammer data

To assess the physical fidelity of the high-quality data recorded from the fluidic hammer, a detailed kinematic analysis was performed, followed by an independent benchmark validation.

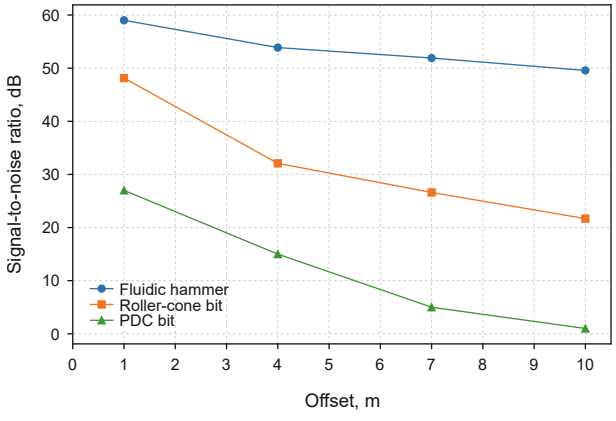


Fig. 6. SNR as a function of offset for the three seismic sources. All curves are calculated from the experimental data recorded at offsets of 1, 4, 7, and 10 m.

The primary method for travel-time determination relied on the exceptional repeatability of the fluidic hammer's source wavelet. As a prerequisite, this high repeatability was confirmed by cross-correlating a 100 ms reference wavelet (from the 1 m offset) with the signals from all other offsets. This process consistently yielded sharp, unambiguous peaks for both near and far distances, as shown in Fig. 7. By picking the time lags corresponding to these peaks, we precisely determined the relative travel times for our primary dataset.

To independently validate the accuracy of this cross-correlation methodology, the data from the separate benchmark experiment was used. The clean waveforms from this experiment, presented in Fig. 8, allowed for unambiguous manual picking of the first arrivals, yielding a set of ground-truth absolute travel times. For a direct and robust comparison, these absolute travel times were converted into relative travel times by subtracting the travel time of the 1 m reference sensor.

Fig. 9 presents the final comparative velocity inversion, plotting the data from the primary fluidic hammer experiment against the data from the independent benchmark experiment. The results demonstrate exceptional agreement. Linear regression on the fluidic hammer data (cross-correlation) yields an apparent velocity of 3001 m/s ($R^2 = 0.9893$), while the benchmark data (direct picking) yields a nearly identical velocity of 3064 m/s ($R^2 = 0.9982$). It should be noted that the minor deviation observed at the 10 m offset is likely attributed to local inhomogeneity in the concrete floor, such as subsurface

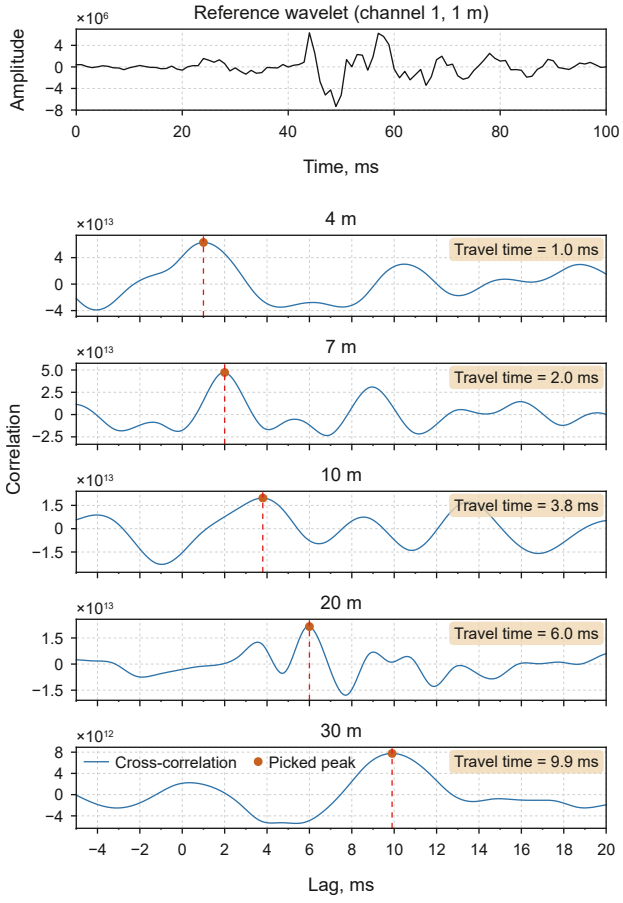


Fig. 7. Travel-time picking for the fluidic hammer source using cross-correlation. The reference wavelet from the 1 m trace (top panel) is correlated with signals from other offsets. The peaks of the correlation functions (orange circles) determine the precise relative travel times for the primary dataset.

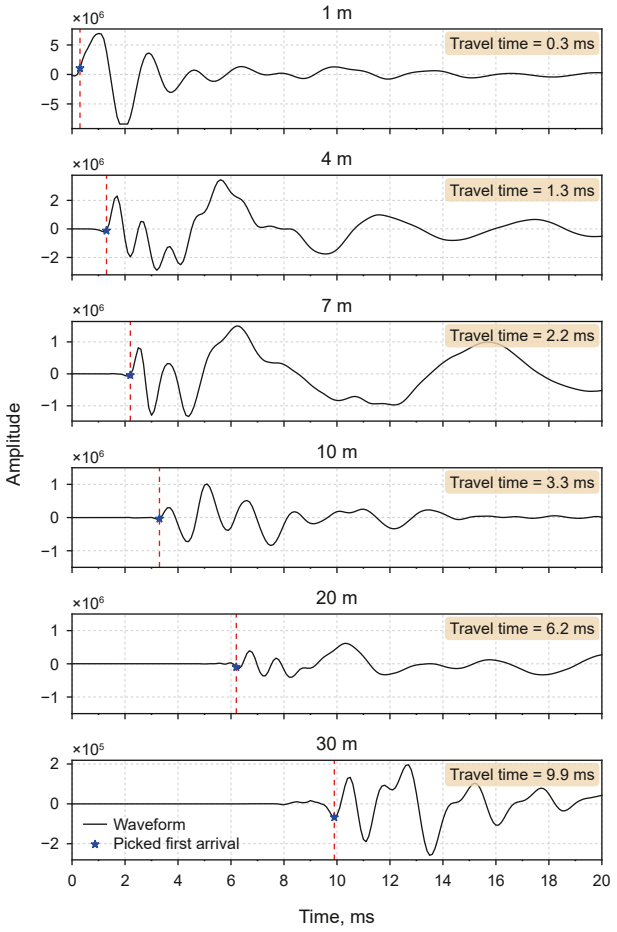


Fig. 8. Benchmark experiment using a hammer source with direct first-arrival picking. Waveforms were recorded in a separate experiment using an instrumented hammer. The blue stars indicate the manually picked first arrivals, yielding a set of absolute travel times for independent validation.

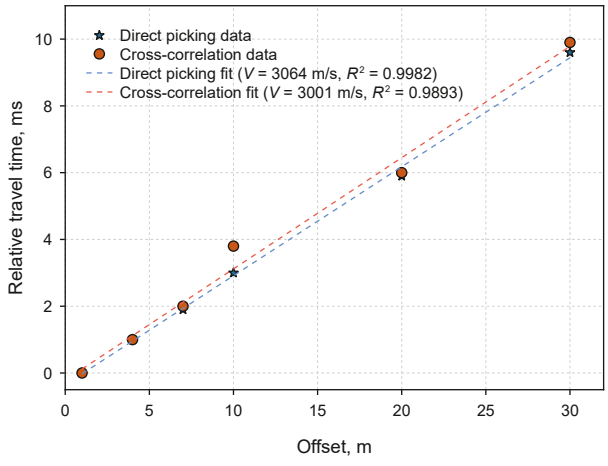


Fig. 9. A direct comparison of relative travel times obtained from two independent experiments. Blue stars represent data from the benchmark hammer experiment (direct picking), while orange circles represent data from the primary fluidic hammer experiment (cross-correlation). The excellent agreement between the two datasets robustly validates the kinematic fidelity of the fluidic hammer data and the cross-correlation methodology.

reinforcement or micro-variations in material density. Furthermore, compared to direct first-arrival picking, the cross-correlation method is more sensitive to waveform distortions caused by such local scattering, leading to the observed slight phase lag. However, the high linearity of the overall trend ($R^2 > 0.98$) confirms that the method is robust against such local anomalies. This excellent consistency between the results of two independent experiments—using different sources and processing workflows—provides powerful validation. Furthermore, both the velocity derived from the fluidic hammer data (3001 m/s) and the benchmark hammer data (3064 m/s) are in excellent agreement with the P-wave velocity of 3100 m/s, which was measured independently via ultrasonic testing on a core sample from the concrete floor. This triple confirmation robustly verifies that the cross-correlation methodology applied to the fluidic hammer data accurately captures the true kinematic properties of the wavefield.

3.4. *Performance quantification: controllability and spectral stability*

A fundamental advantage of the fluidic hammer over passive drill-bit sources is the ability to control its output. Our experiments quantitatively demonstrate this key performance characteristic. The quality of the radiated signal, represented by the SNR, was found to be a directly controllable parameter. As shown in Fig. 10, the SNR at every offset systematically increases with the pump flow rate, confirming that signal quality can be effectively and predictably enhanced by adjusting operational parameters.

Furthermore, the energy output and spectral stability of the source were quantified as a function of flow rate (Fig. 11). A strong linear relationship (with a coefficient of determination, $R^2 = 0.9360$) is observed between the source's peak energy output and the operational flow rate (Fig. 11(a)). This provides direct quantitative proof that the energy output is precisely controllable. Complementing this, the source exhibits exceptional spectral

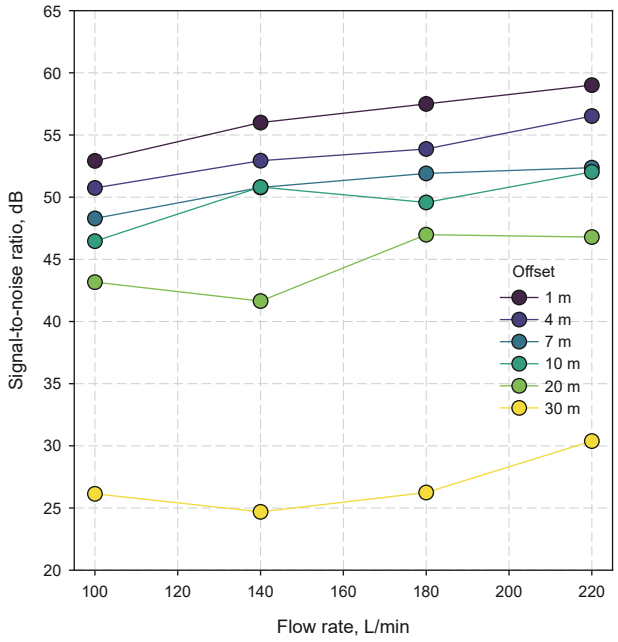


Fig. 10. Controllability of signal quality. The SNR is plotted as a function of flow rate for each individual offset. The clear positive correlation for all distances confirms that signal quality can be predictably controlled.

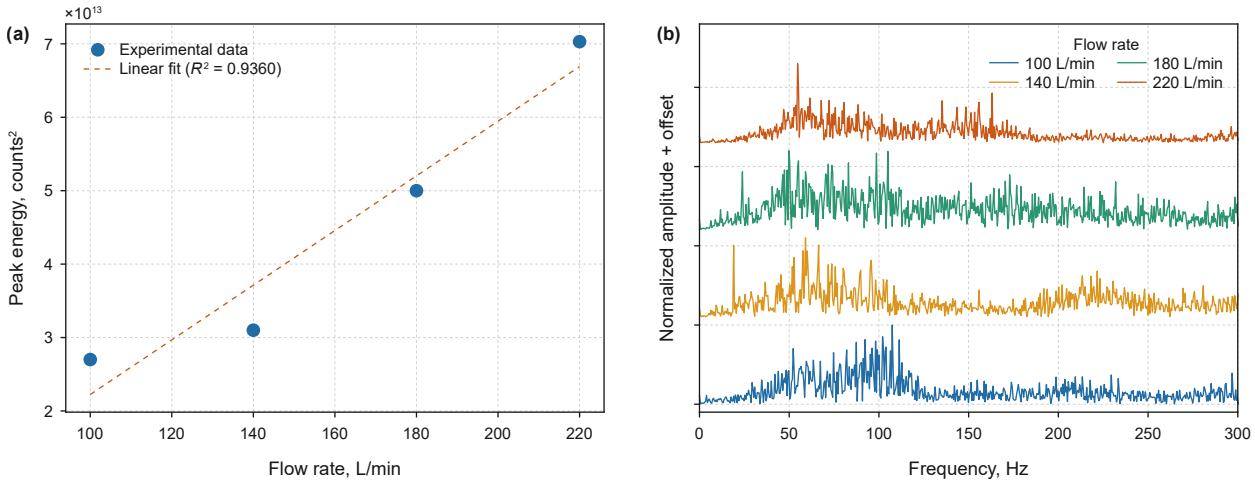


Fig. 11. Quantitative demonstration of source controllability and stability. (**a**) A strong linear correlation (R^2 = 0.9360) between peak energy and flow rate. (**b**) Normalized amplitude spectra for four different flow rates, showing remarkable consistency in spectral shape despite varying energy levels.

stability. Despite the significant variations in energy output, the normalized amplitude spectra for the flow rates of 140, 180, and 220 L/min are remarkably consistent in their overall shape and dominant frequency band (Fig. 11(b)). The distinct spectral characteristic observed at the 100 L/min flow rate is attributed to the transition from a short-stroke startup mode to full-stroke operation. At this threshold flow rate, the hydraulic energy is insufficient to drive the piston through its full designed stroke (110 mm), leading to higher-frequency, low-energy oscillations (short-stroke flutter). As the flow rate increases to 140 L/min and above, the hammer achieves stable full-stroke impacts, resulting in a consistent dominant frequency band (~50 Hz) and a linear increase in radiated energy. This combination of controllable energy and a stable, repeatable signature is a critical prerequisite for advanced, high-fidelity seismic processing techniques such as quantitative time-lapse analysis and deconvolution.

Beyond spectral consistency, the source's kinematic and waveform stability was rigorously evaluated to further confirm its stability. A cross-correlation analysis was performed between the signals recorded at 1 and 4 m offsets under the four distinct operational flow rates. The results, presented in Fig. 12, provide compelling evidence of the fluidic hammer's exceptional stability. Qualitatively, the cross-correlation functions exhibit a highly consistent wavelet signature across all energy levels, demonstrating the robustness of the physical percussion mechanism. Quantitatively, the source's stability is even more striking: The travel time derived from the correlation peak remains precisely constant at 1.0 ms, irrespective of the flow rate. This remarkable kinematic stability, even under significantly varying energy outputs, confirms that the fluidic hammer is a highly repeatable source, making it an ideal candidate for high-fidelity quantitative seismic studies that demand a consistent source signature. The 3 m geometric distance between the 1 and 4 m sensors, combined with the apparent concrete velocity of approximately 3000 m/s, yields a theoretical travel-time difference of approximately 1.0 ms, which is in excellent agreement with the observed 1.0 ms, thus confirming the mathematical-physical consistency of the data.

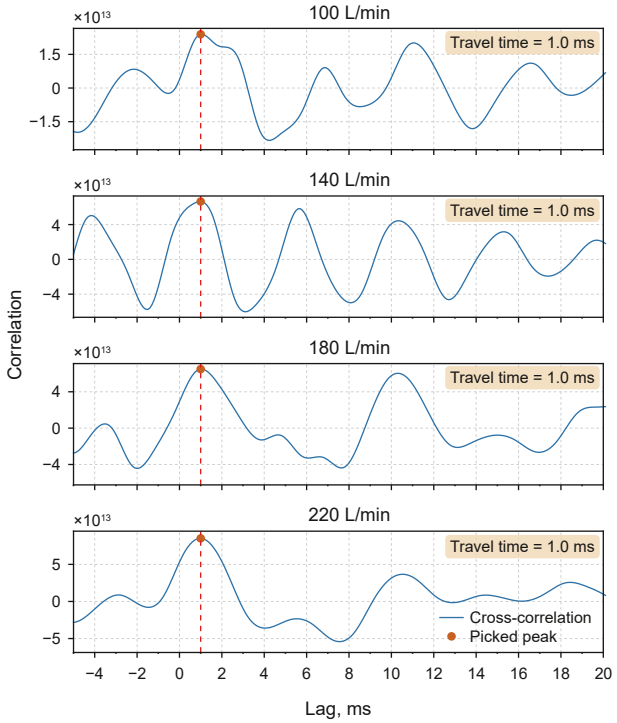


Fig. 12. Kinematic and waveform stability of the fluidic hammer source under varying energy levels. The plots show the cross-correlation between the 1 and 4 m sensor signals for four different flow rates. Despite the significant change in energy, the wavelet signature remains consistent, and the travel time is precisely stable at 1.0 ms, confirming the source's high degree of repeatability.

4. Discussion

This study provides the first systematic, quantitative comparison between the seismic signals generated by a fluidic hammer and those from conventional roller-cone and PDC bits under controlled laboratory conditions. While previous studies have characterized individual drill-bit sources or impact-based tools, this work moves beyond isolated characterizations to provide a direct, evidence-based evaluation of their relative performance. Our results robustly demonstrate that the fluidic hammer mechanism offers a substantial performance improvement over traditional passive drill-bit sources, establishing a quantitative benchmark for source performance in SWD (Ivandic et al., 2022).

The macroscopic comparison revealed a significant disparity in radiated energy, with the fluidic hammer producing peak energies approximately 12.2 and 809.3 times greater than the roller-cone

and PDC bits, respectively. This high energy output, combined with its broad frequency spectrum (Fig. 4), directly addresses two primary limitations of conventional SWD: limited signal penetration and low resolution. These advantages collectively result in a superior SNR that not only decays much more slowly with distance (Fig. 6) but also maintains an impressive ~30 dB even at the maximum offset of 30 m under high-energy conditions (Fig. 10), which stands in stark contrast to the performance of passive drill-bit sources under typical field conditions (Rector and Marion, 1991).

However, to ensure these impressive performance metrics are not just artifacts but are physically meaningful, the fidelity of the analysis methodology itself was rigorously validated. Crucially, the reliability of the kinematic data derived from the fluidic hammer was confirmed through a comparative analysis against an independent benchmark experiment using a traditional instrumented hammer (Figs. 8 and 9). This validation revealed a high degree of consistency, with the velocities derived from the fluidic hammer (3001 m/s) and the benchmark test (3064 m/s) being in excellent agreement. Furthermore, both seismically-derived velocities align closely with the 3100 m/s P-wave velocity measured from a physical core sample of the concrete floor. This “triple confirmation” provides a robust foundation for all quantitative claims made in this study, confirming the physical fidelity of the measurements.

With the source’s superiority and the method’s reliability established, the analysis then revealed the fluidic hammer’s most transformative advantages over passive sources: its unique controllability and stability. This study reveals a new paradigm where the peak energy output of the fluidic hammer is directly and linearly related to a single engineering parameter—the flow rate (Fig. 11(a)). This transforms the source from an incidental byproduct of rock destruction into a calibratable, quantifiable tool. This controllability is complemented by exceptional stability. Despite significant variations in energy, the wavelet signature and its corresponding travel time remain remarkably stable (Fig. 12), and the spectral signature is highly consistent across all energy levels (Fig. 11(b)). This level of stability is unattainable by pseudo-random sources like conventional bits and is a critical prerequisite for advanced quantitative analyses, such as time-lapse reservoir monitoring.

The development of such a high-fidelity, controllable while-drilling source has profound implications, particularly when synergized with modern high-density acquisition systems like distributed acoustic sensing (DAS) (Bakulin et al., 2020). While DAS offers unprecedented spatial sampling, its full potential is often limited by the quality of passive sources. The energetic, broadband, and highly repeatable signals generated by the fluidic hammer provide an ideal input for DAS-based applications. The high-frequency characteristics (>100 Hz) are especially critical, as the fidelity of a DAS measurement is fundamentally linked to the ratio of the seismic wavelength to the system’s gauge length, with shorter wavelengths being necessary for high-resolution imaging (Dean et al., 2017). This synergy could enable applications such as real-time, high-resolution vertical seismic profiling (VSP), a technique used in diverse applications like site monitoring (Egorov et al., 2018), and look-ahead-of-the-bit imaging with improved clarity.

Finally, the limitations of this study must be acknowledged. The experiments were conducted under controlled laboratory conditions using a homogeneous concrete medium, which differs significantly from the heterogeneous and highly attenuative environment typical of real geological formations. Additionally, the surface-based linear geophone array, while effective for quantifying surface propagation, could not capture the full three-dimensional downward radiation characteristics essential for lateral imaging. Transitioning to field applications also introduces operational complexities, such as the need for robust downhole cooling and erosion protection, and the controllability of the fluidic oscillator under varying mud properties remains to be validated. To address these gaps, future work will focus on pilot tests utilizing DAS or multi-azimuth VSP arrays. These field trials will serve the dual purpose of mapping the complete 3D radiation response and calibrating the source performance under operational drilling conditions. In parallel with these validation efforts, research will also target the optimization of the hammer's design to further enhance its efficiency and frequency bandwidth, alongside the development of real-time processing workflows that can fully leverage the deterministic nature of this source.

5. Conclusions

In this study, a systematic laboratory experiment was conducted to quantitatively characterize a fluidic hammer as a high-performance while-drilling seismic source, through a direct comparison with conventional roller-cone and PDC bits. The experimental results demonstrate the comprehensive superiority of the fluidic hammer. In terms of fundamental performance, it consistently generates a signal with significantly higher energy (approximately 12.2 times that of the roller-cone bit and over 809.3 times that of the PDC bit), a broader effective frequency band, superior wavelet repeatability, and a higher signal-to-noise ratio (SNR) that decays more slowly with distance than its conventional counterparts.

Crucially, the fidelity and accuracy of this entire methodology were first substantiated by an independent benchmark experiment, confirming that the fluidic hammer system, coupled with cross-correlation processing, reliably captures the true kinematics of the wavefield. Building on this validated foundation, this work provides strong, quantitative evidence for the fluidic hammer’s most distinctive advantage over passive sources: its controllability. A strong linear relationship was established between the operational flow rate and the resulting peak energy. This controllability is complemented by exceptional stability across all tested energy levels, demonstrated by a consistent spectral signature, a repeatable wavelet shape, and an unwavering kinematic response. This transforms the drill-bit source from an incidental, unpredictable noise generator into a calibratable tool—where both the energy output level and the source signature are predictable functions of the hydraulic flow rate. This shift confers quasi-active characteristics to the source, defined here as the ability to generate deterministic, periodic signals with controllable parameters despite being powered by the drilling process.

These combined findings—high energy, high-fidelity, and unique controllability—confirm that the fluidic hammer source mechanism can effectively overcome the critical flaws of traditional seismic-while-drilling (SWD). This provides a solid physical basis and a viable technological pathway for the development of next-generation, quantitative subsurface imaging techniques, such as real-time look-ahead-of-the-bit imaging and time-lapse reservoir monitoring.

CRediT authorship contribution statement

Bo-Yao Zhang: Writing – original draft, Software, Methodology, Investigation, Conceptualization. **Jian-Ming Peng:** Writing – review & editing, Resources, Methodology. **Dong Ge:** Writing – review & editing, Validation, Resources, Conceptualization.

Conflict of interest

The authors declare that they have no known competing financial interests or personal relationships that could have appeared to influence the work reported in this paper.

Acknowledgments

This work was supported in part by the Special Fund of the Key Laboratory of Geophysical Exploration Equipment, Ministry of Education (Jilin University) (Project No. GEIOF2023002).

References

Aki, K., 1957. Space and time spectra of stationary stochastic waves, with special reference to microtremors. Bull. Earthq. Res. Inst. 35, 415–456.
Anchliya, A., 2006. A review of seismic-while-drilling (SWD) techniques: A journey from 1986 to 2005. In: SPE Europec/EAGE Annual Conference and Exhibition. SPE 100352–MS. https://doi.org/10.2118/100352-MS.
Bakulin, A., Silvestrov, I., Pevzner, R., 2020. Surface seismics with DAS: An emerging alternative to modern point-sensor acquisition. Lead. Edge 39 (11), 808–818. https://doi.org/10.1190/tle39110808.1.
Bendat, J.S., Piersol, A.G., 2000. Random Data: Analysis and Measurement Procedures. Wiley, New York.
Birnie, C., Liu, S., AlDawood, A., et al., 2024. Self-supervised denoising at low signal-to-noise ratios: A seismic-while-drilling application. Lead. Edge 43 (7), 436–443. https://doi.org/10.1190/tle43070436.1.
Bracewell, R.N., 2000. In: The Fourier Transform and Its Applications, third ed. McGraw-Hill, Boston.
Brett, J.F., Warron, T.M., Bohr, S.M., 1990. Bit whirl—a new theory of PDC bit failure. SPE Drill. Eng. 5 (4), 275–281. https://doi.org/10.2118/19571-PA.
Dean, T., Cuny, T., Hartog, A.H., 2017. The effect of gauge length on axially incident P-waves measured using fibre optic distributed vibration sensing. Geophys. Prospect. 65 (1), 184–193. https://doi.org/10.1111/1365-2478.12419.
Egorov, A., Bóna, A., Pevzner, R., et al., 2018. Application of time-lapse full waveform inversion of vertical seismic profile data for the identification of changes introduced by CO_2 sequestration. ASEG Extended Abstracts 2018 (1), 1–5. https://doi.org/10.1071/ASEG2018abW8_2B.
Ge, D., Peng, J., Li, B., et al., 2022. On the switching mechanisms and output response of an output-fed fluidic oscillator for fluidic hammer over full stroke. Sensor Actuator Phys. 347, 113972. https://doi.org/10.1016/j.sna.2022.113972.
Haldorsen, J.B.U., Miller, D.E., Walsh, J.J., 1995. Walk-away VSP using drill noise as a source. Geophysics 60 (4), 978–997. https://doi.org/10.1190/1.1443863.
Ivandic, M., Kaslilar, A., Juhlin, C., 2022. Subsurface seismic imaging with a hammer drilling source at an exploration drilling test center in Örebro, Sweden. Adv. Geosci. 56, 163–169. https://doi.org/10.5194/adgeo-56-163-2022.
Jiang, Y.D., 2004. A review of seismic-while-drilling technology. Geophys. Prospect. Pet. 43 (2), 202–208. https://doi.org/10.3969/j.issn.1000-1441.2004.02.024 (in Chinese).
Miranda, F., Aleotti, L., Abramo, F., et al., 1996. Impact of the seismic while drilling technique on exploration wells. First Break 14 (2). https://doi.org/10.3997/1365-2397.1996004.
Miranda, F., Poletto, F., Abramo, F., et al., 1999. SWD surface and downhole pilot recording to improve PDC bit signals. In: 61st EAGE Conference and Exhibition. https://doi.org/10.3997/2214-4609.201407779.
Naville, C., Serbutoviez, S., Throo, A., et al., 2004. Seismic while drilling (SWD) techniques with downhole measurements, introduced by IFP and its partners in 1990-2000. Oil Gas Sci. Technol. 59 (4), 371–403. https://doi.org/10.2516/ogst:2004027.
Poletto, F., 2005. Energy balance of a drill-bit seismic source, part 1: Rotary energy and radiation properties. Geophysics 70 (2), T13–T28. https://doi.org/10.1190/1.1897038.
Poletto, F., Miranda, F., 2004. Seismic While Drilling: Fundamentals of Drill-Bit Seismic for Exploration. Pergamon, Oxford.
Rector, J.W., 1990. System for Reducing Drill String Multiples in Field Signals. European Patent EP0349262.
Rector, J.W., Marion, B.P., 1991. The use of drill-bit energy as a downhole seismic source. Geophysics 56 (5), 628–634. https://doi.org/10.1190/1.1443079.
Rector, J.W., Hardage, B.A., 1992. Radiation pattern and seismic waves generated by a working roller-cone drill bit. Geophysics 57 (10), 1319–1333. https://doi.org/10.1190/1.1443199.
Reppert, P.M., 2013. Seismic while drilling (SWD) with a rotary percussive sounding system (RPSS). J. Environ. Eng. Geophys. 18 (3), 169–182. https://doi.org/10.2113/JEEG18.3.169.
Soma, N., Utagawa, M., Seto, M., et al., 2004. Identification of subsurface structures using the seismic-while-drilling technique. Int. J. Rock Mech. Min. Sci. 41 (1), 165–173. https://doi.org/10.1016/S1365-1609(03)00081-9.
Stein, S., Wysession, M., 2009. An Introduction to Seismology, Earthquakes, and Earth Structure. Wiley, Oxford.
Su, Y.N., Xu, Y., Sheng, L.M., et al., 2010. Review on study progress of seismic while drilling technology. Oil Drilling & Production Technology 32 (5), 1–7. https://doi.org/10.13639/j.odpt.2010.05.033 (in Chinese).
Sun, B., Bóna, A., Zhou, B., et al., 2015. A comparison of radiated energy from diamond-impregnated coring and reverse-circulation percussion drilling methods in hard-rock environments. Geophysics 80 (4), K13–K23. https://doi.org/10.1190/geo2014-0344.1.
Wilczynski, Z., Kaslilar, A., Ivandic, M., et al., 2023. Drill-bit position monitoring using seismic-while-drilling data; numerical and field examples from Sweden. Geophys. Prospect. 71 (7), 1338–1355. https://doi.org/10.1111/1365-2478.13330.
Yokota, T., Onishi, K., Karasawa, H., et al., 2004. Seismic while drilling: Basic experiments using a percussion drill as an energy source. Explor. Geophys. 35 (4), 255–259. https://doi.org/10.1071/EG04255.
Zhang, M.K., Zhao, Q.H., Luo, B., et al., 2022. Review of the drill bit seismic while drilling technology. Prog. Geophys. 37 (4), 1677–1688. https://doi.org/10.6038/pg2022FF0514 (in Chinese).
Zhou, B., Mason, I., Greenhalgh, S., et al., 2015. Seeing coal-seam top ahead of the drill bit through seismic-while-drilling. Geophys. Prospect. 63 (1), 166–182. https://doi.org/10.1111/1365-2478.12172.